Interferences in the photoionization of water molecules

Lara Martini[1], Diego I R Boll[1] & Omar A Fojón[1,2]

[1] Grupo de Colisiones Atómicas, Instituto de Física Rosario (CONICET-UNR), 27 de febrero 210 bis, 2000 Rosario, Santa Fe, Argentina

[2] Escuela de Ciencias Exactas y Naturales (FCEIA-UNR), Pellegrini 250, 2000 Rosario, Santa Fe, Argentina

E-mail: martini@ifir-conicet.gov.ar

February 2018

Abstract. We study theoretically the photoionization of water molecules by monochromatic and linearly polarized radiation. The final state wavefunctions are given by Coulomb continuum wavefunctions and the water molecule bound states are represented using linear combinations of Slater type orbitals located on the centers of the molecule. We obtain total and differential cross sections. We compare them with more elaborated theoretical results and experiments obtaining a very good agreement in particular at enough high energies where there is a lack of predictions. We put in evidence three-center interference effects not only in the total cross sections but also we show that these effects may be detected in a direct way in the angular distributions of photoelectrons corresponding to randomly oriented molecules. In particular, we find that the interference effects under certain conditions may provoke a partial suppression of the emission of photoelectrons in the classical direction given by the polarization vector.

PACS numbers: 33.80.-b, 33.90.+h

Keywords: photoionization, water, three-center effects, interferences

Submitted to: *J. Phys. B: At. Mol. Opt. Phys.*

1. Introduction

Ionization of water molecules is of interest in many domains such as radiochemistry and radiobiology as living cells are composed mostly by water. As a matter of fact, ionization of water molecules by massive particles was studied in several experimental and theoretical works as well as for photon impact (see for instance [1, 2, 3, 4, 5, 6, 7, 8, 9, 10, 11]).

The theoretical treatment of these reactions is rather involved if the nuclear degrees of freedom of the water molecule must be taken into account together with the proper treatment of the continuum states in the final channel of the reaction. Elaborated methods were developed to obtain cross sections for photoionization of water. For instance, Stener *et al* [2] studied the reaction within the framework of the Density Functional Theory (DFT) with different exchange-correlation potentials having the correct asymptotic behaviour and they obtain cross sections up to approximately 70 eV. However, theoretical cross sections at higher energies are needed to contrast with experiments to back research for instance on matter irradiation.

Considering the complexities of the problem, approximations are necessary to obtain observables of the reaction especially at high photon impact energies. In particular, at these energies one can simplify the problem by assuming that the reaction occurs in a lapse much smaller than the typical vibrational, rotational and relaxation times of the molecule. Taking into account that the absorption of a photon of a definite frequency and the subsequent emission of a photoelectron is an (ultra) fast process, then we may assume that photoionization is produced at a fixed-in-space orientation of the molecule. As explained in previous works [12, 13], this fixed nuclei approximation is reasonable if one is not interested in a vibrational analysis of the residual molecular ion except very close to the threshold or in the vicinity of resonance states. Therefore, the molecule can be taken as frozen at the equilibrium configuration during the collision time as a well grounded approximation. Moreover, the single active independent electron approximation can be applied. All these assumptions were employed with success in previous works (see for instance [14, 15] and references there in), rendering the problem tractable to obtain reliable cross sections. In addition, bound states for the water molecule may be well described by quantum chemistry methods. In particular, basis made of linear combinations of Slater type orbitals (STO) or Gaussian type ones are commonly used and accessible through available codes. In this way, bound states energies may be obtained with a high degree of precision. Besides, approximations such as the CNDO (*Complete Neglected of Differential Overlap*) [16] may bring reasonable autoenergies. In the computations of energy eigenvalues of this approximation, the overlapping integrals between the atomic orbitals are completely neglected. Even if the bound states are accessible through a wide variety of standard methods, the continuum states of the active electron in the final channel still remains a challenge to describe in a realistic way the ionization of complex molecules. The multicenter nature of the residual target introduces complications in the theoretical descriptions.

Then, approximations taking into account the screening provoked by the passive electrons of the molecule may be employed. Gozem *et al* [1] employed final continuum states represented by Coulomb waves describing the interaction between the active electron and the residual target. The influence of the passive electrons on the reaction is included through the use of different charges Z_{ef} for the Coulomb

waves for many molecules.

Recently, we performed total cross sections calculations for several orbitals of the water molecules [17]. We developed a first order model describing the bound states by using monocentric Moccia's wavefunctions. We employed a Coulomb Continuum (CC) approximation in which the final state of the ejected electron is described through a Coulomb wavefunction with a charge that describes the screening of the nuclear charges of the molecule. We were able to obtain analytical expressions for the matrix transition elements. We observed a very good agreement with the available experiments especially at high impact energies where there is a lack of theoretical results.

In this work, we go a step further. Our main objective is to analyze the effect provoked by the three-center structure of the water molecule on the photoionization process, especially those produced by the coherent emission from the molecular centers. Therefore, we obtain differential and total cross sections within the dipole approximation including in an approximate way the multicenter geometry of the water molecule. The ground state of water is described by a linear combination of Slater orbitals centered on each atom of the molecule whereas the continuum states are described through Coulomb wavefunctions with different distorted charges. The coherent emission was actively studied in the last years particularly for diatomic molecules [21]. We explore here the case of water as a benchmark for the study of interferences in the photoelectron spectra induced by coherent emission. In previous works [10, 11], photoionization of water from the localized oxygen core was studied and interferences produced by recollisions of the emitted electron with the hydrogens of the molecule were analyzed. These processes include necessarily second order terms to describe the emission and subsequent dispersion by the H centers. On the contrary, we focus here in the valence electrons of water, especially those occupying ligand orbitals in which the electrons are shared by the atoms composing the molecule. We look for interference effects coming from the coherent emission from these orbitals delocalized over the centers of the molecule for which recollisions may be disregarded [18].

Otherwise stated atomic units are used.

2. Theory

2.1. Coulomb Continuum (CC) model

In the dipole approximation, the transition matrix amplitude for photoionization by a photon of frequency ω within the velocity *gauge* reads,

$$M_{ph} = -\mathrm{i}\langle\psi_f|\mathbf{e}\cdot\nabla|\psi_b\rangle, \tag{1}$$

where ψ_b denotes the initial target bound wavefunction of the electron in the initial channel and ψ_f represents the electron continuum state in the final channel. Moreover, $\mathbf{e}$ is the polarization vector of the incident radiation.

Within a single active independent electron model in which the active electron is ionized and the passive electrons remain in their initial electronic configurations, the final continuum state of the active electron is chosen as,

$$\psi_f(\mathbf{r}) = (2\pi)^{-3/2} e^{\mathrm{i}\mathbf{k}_e\cdot\mathbf{r}} N_{k_e} G(\mathbf{r})\,, \tag{2}$$

where $\mathbf{r}$ is the active electron coordinate, $\mathbf{k}_e$ is the final electron momentum, and N_{k_e} is the normalization factor given by,

$$N_{k_e} = e^{\pi\nu/2}\Gamma(1+\mathrm{i}\nu)\,, \tag{3}$$

with $\nu = Z_{ef}/k_e$ the Sommerfeld parameter where Z_{ef} is the residual charge of the target, and G is the hypergeometric confluent function,

$$G(\mathbf{r}) = {}_1F_1(-\mathrm{i}\nu; 1; -\mathrm{i}\,(k_e r + \mathbf{k}_e\cdot\mathbf{r}))\,. \tag{4}$$

The final wavefunction of the CC model (2) takes into account the Coulomb interaction of the electron with the residual target in the final channel of the reaction. It was shown that this interaction must be included for to describe the photoionization reaction with neutral targets in a proper way [1, 19, 20, 17]. The choice $Z_{ef} = 1$ corresponds to the asymptotic value of the residual target charge at sufficiently large distances from the target. Alternatively, distorted charges different from unity may be taken to include in an approximate way the screening of the passive electrons in the dynamics of the reaction [1, 21].

2.2. Ground state of water

In its ground state, the water molecule has the following electronic configuration,

$$(1a_1)^2\ (2a_1)^2\ (1b_2)^2\ (3a_1)^2\ (1b_1)^2. \tag{5}$$

In this work, we represent the initial bound orbitals (ψ^j) of the water molecule in its ground state by means of linear combinations of STO centered on the oxygen and hydrogen atoms,

$$\psi^j = \sum_i \sum_\mu^{\mathbb{N}}\ c_{i\mu}^j f_\mu\left(\mathbf{r}_i'\right). \tag{6}$$

In the last expression, $c_{i\mu}^j$ is a real coefficient and i identifies the centers of the molecule (i =0, 1 and 2 for the O, H_a and H_b center respectively, see figure 1). The position vector of an electron as measured from the center i is denoted by $\mathbf{r}_i'$, f_μ is the atomic orbital basis function where μ identifies the different elements of the basis set (in this work, $\mu \equiv 1s$, $2s$, $2p_x$, $2p_y$, $2p_z$, $3d_{z^2}$, $3d_{xz}$, $3d_{yz}$, $3d_{x^2-y^2}$ and $3d_{xy}$) with total number of elements given by $\mathbb{N}$. The f_μ may be expressed as linear combinations of STO which in turn are given by,

$$\phi_{n,l,m}(r,\theta,\varphi) = \left[\frac{(2\xi)^{2n+1}}{(2n)!}\right]^{1/2} r^{n-1}e^{-\xi r}Y_{l,m}(\theta,\varphi)\,, \tag{7}$$

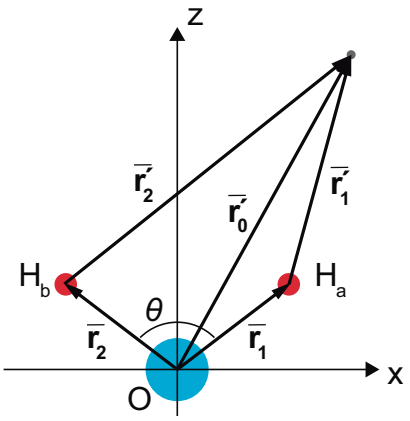

Figure 1: Geometry of the ground state of the water molecule. The origin of coordinates is located at the O nuclei and the plane of the molecule coincides with the xz plane with the H atoms pointing up. The vectors $\mathbf{r}'_1$ and $\mathbf{r}'_2$ point towards the H_a and H_b nuclei respectively from the origin. The bond angle is $\theta = 104°27'$ and the $O-H$ distances are $r_1 = r_2 = 1.811$. The vectors $\mathbf{r}'_0$, $\mathbf{r}'_1$ and $\mathbf{r}'_2$ point towards the active electron from the O, H_a and H_b nuclei, respectively.

Table 1: Orbital energies E_b for the basis sets employed in this work compared to the experimental ones taken from [22].

	$1a_1$	$2a_1$	$1b_2$	$3a_1$	$1b_1$
Basis set I	-20.5559	-1.2850	-0.6242	-0.4661	-0.4026
Basis set II	-20.5421	-1.3534	-0.7099	-0.5638	-0.5077
Basis set III	-20.5541	-1.3356	-0.7153	-0.5840	-0.5130
Basis set IV	-20.5654	-1.3392	-0.7283	-0.5950	-0.5211
Experimental value	-19.8419	-1.1838	-0.6765	-0.5404	-0.4632

where n, l, m are the usual quantum numbers, r, θ, φ represents the spherical coordinates, and $Y_{l,m}(\theta, \varphi)$ are the spherical harmonics.

We employ four basis sets [23]. The first one is given by the minimal basis, *i.e.*, a basis compound of seven ($\mathbb{N} = 7$) f_μ representing the occupied orbitals of the hydrogen and oxygen atoms. In the second one, an additional $2p$ orbital for the oxygen is added. In the third one, an additional $1s$ orbital for the hydrogen and additional $2s$, $2p$ and $3d$ orbitals for the oxygen are included. Finally, in the fourth one, additional $2s$ and $2p$ orbitals for the hydrogen and additional $2s$, $2p$ and $3d$ orbitals for the oxygen are considered. The water orbital energies for each set as well as the experimental ones [22] are given in table 1.

2.3. Transition matrix elements

We obtain the matrix transition element for a definite initial orbital of water ψ^j (given by (6)) within the framework of an effective center approximation [18]. In this approximation we consider that the emission of the electron is produced mainly in the neighborhoods of either molecular center.

Then, by taking $\psi_b = \psi^j$ in (1) and applying the effective center approximation (see Appendix A), we have the following expression,

$$M_{ph}^{j} \sim M_{ph}^{j,O}\left(Z_{ef}^{j,O}\right) + g_1\, M_{ph}^{j,H_a}\left(Z_{ef}^{j,H_a}\right) + g_2\, M_{ph}^{j,H_b}\left(Z_{ef}^{j,Hb}\right), \tag{8}$$

where

$$g_i(\mathbf{r}_i) = e^{-\mathrm{i}\mathbf{k}_e\cdot\mathbf{r}_i}, \tag{9}$$

with $i = 1, 2$ and where $M_{ph}^{j,i}\left(Z_{ef}^{j,i}\right)$ is the matrix transition element for the center labelled i given by (A.3),

$$\begin{aligned} M_{ph}^{j,i} =& -\mathrm{i}\langle\psi_f|\mathbf{e}\cdot\nabla|\sum_{\mu}^{\mathbb{N}} c_{i\mu}^{j} f_\mu\left(\mathbf{r}_i'\right)\rangle \\ =& \sum_{\mu}^{\mathbb{N}} c_{i\mu}^{j}\left(-\mathrm{i}\langle\psi_f|\mathbf{e}\cdot\nabla|f_\mu\left(\mathbf{r}_i'\right)\rangle\right), \end{aligned} \tag{10}$$

where $f_\mu\left(\mathbf{r}_i'\right)$ is a linear combination of STO. Then, $M_{ph}^{j,i}$ is expressed as a linear combination of matrix transition elements for an individual STO. Analytical expressions for these matrix transition elements are given in Appendix B. Moreover, $Z_{ef}^{j,i}$ are the charges for the final continuum state. These charges are chosen according to which center we assume the photoelectron is ionized.

In this way, the matrix transition element for a given initial bound orbital of water given by equation (8) may be interpreted as the coherent sum of three matrix elements (times an adequate factor) describing coherent emission from each molecular center. The factors g_i $(i = 1, 2)$ may be considered then as traslational factors that account for the internuclear displacements from the O center (origin of coordinates) and the H_a or H_b center (see figure 1).

Then, disregarding recollisions between centers, the dominant physical mechanisms involved in the photoemission will depend critically on the localization degree of the orbital from which electrons are emitted. For instance, if ionization takes place from an orbital located on only one center of the molecule, the sum will not include terms from the remaining centers. This is the case for photoionization from the $1b_1$ non-ligand orbital of water located on the oxygen atom.

On the contrary, if photoemission takes place from a ligand orbital where the electrons are shared by and, consequently, delocalized between centers corresponding to the oxygen and hydrogen atoms, then the matrix element will certainly include terms from all centers leading to the phenomenon of coherent emission [18].

2.4. Cross sections

Differential cross sections *per electron* for a definite orientation of the molecule as a function of the photon energy and the solid angle of the ejected electron for a given initial bound orbital $\psi_b = \psi^j$ may be obtained as [24],

$$\frac{d\sigma^j(\omega)}{d\Omega_e d\Omega_{Euler}} = \frac{4\pi^2 \alpha k_e}{\omega} |M^j_{ph}|^2, \tag{11}$$

where M^j_{ph} is the matrix transition element defined in the preceding subsection, α is the fine structure constant, ω is the frequency of the incident photon, k_e is the magnitude of the ejected electron momentum, $d\Omega_{Euler}$ defines the orientation of the molecule in terms of its Euler angles, and $d\Omega_e = sin\theta_e \, d\theta_e \, d\varphi_e$ being Ω_e the solid angle of the ejection direction as measured in the coordinate system of figure 1.

Integrating over all directions of ejection, one obtains cross sections for a definite orientation of the molecule as a function of the photon energy,

$$\frac{d\sigma^j(\omega)}{d\Omega_{Euler}} = \int d\Omega_e \left(\frac{d\sigma^j(\omega)}{d\Omega_e d\Omega_{Euler}} \right). \tag{12}$$

In many experiments, molecules are randomly oriented. Then, an average over the Euler angles in (12) is needed to obtain averaged total cross sections as a function of the photon energy,

$$\sigma^j(\omega) = \frac{1}{8\pi^2} \int d\Omega_{Euler} \left(\frac{d\sigma^j(\omega)}{d\Omega_{Euler}} \right). \tag{13}$$

Then, the total cross section corresponding to all bound orbitals of the ground state of the water molecule may be obtained as,

$$\sigma(\omega) = \sum_j N_j \, \sigma^j(\omega), \tag{14}$$

where the occupation number for all orbitals is $N_j = 2$.

3. Results

3.1. Total cross sections

We present our total cross sections for the single photoionization of randomly oriented water molecules by photons of frequency ω linearly polarized. We compare our predictions with available theoretical and experimental results. To compare with measurements, we average our cross sections over all orientations of the water molecule, *i.e.*, over all Euler angles of the molecule.

We have verified that results obtained within the length and velocity *gauge* are almost the same in the present energy domain. In relation to the electronic final continuum states, we have considered different charges $Z^{j,O}_{ef}$ and $Z^{j,H_{a,b}}_{ef}$ for the Coulomb function describing the photoelectron in the final channel. On one

hand, we have considered the asymptotic charge value $Z_{ef}^{j,O} = Z_{ef}^{j,H_{a,b}} = 1$. On the other hand, we have considered distorted charges obtained with the Belkić's rule [21] $Z_{ef}^{j,i} = \sqrt{2n_{j,i}^2|E_b^j|}$, where $n_{j,i}$ is the predominant quantum number of the i-th center of the j-th orbital and E_b^j is the experimental energy of the j-th orbital.

In figure 2(a), 2(c) and 2(e), we show our predictions with the different basis sets and the different continuum charges together with experiments for the $1b_1$, $3a_1$ and $1b_2$ orbitals respectively. In all cases, the basis set IV with the Belkić's rule for the distorted charge value is the best choice. In figures 2(b), 2(d) and 2(f), we compare our results for the basis set IV for the $1b_1$, $3a_1$ and $1b_2$ orbitals respectively with previous theoretical curves and experiments.

From inspection of the figure 2(b), it can be seen that our model gives a very good agreement with experiments. We can observe that our calculations with $Z_{ef}^{O} = 1.9250$ and $Z_{ef}^{H_{a,b}} = 1.9250$ (for the $1b_1$, $Z_{ef}^{H_{a,b}}$ is only needed for the basis set IV) agree qualitatively well with the ones by Stener *et al* [2] for photon energies greater than 25 eV where they have almost the same slope. In particular, the best quantitative agreement with our cross sections is observed for the VWN choice with the GS configuration.

In addition, we can also see for the $1b_1$ orbital in figure 2(b) that our cross sections are in very good accordance with the ones obtained with Dyson orbitals [1] in the energy range [35,60] eV. At lower energies, there is some discrepancy. Moreover, our results agree qualitatively with the ones by Hilton *et al* [25] in the energy range [30,40] eV. They applied a simpler approach based on the superposition of atomic processes by using the molecular form of the ground state inversion potential method (GIPM). For the $1b_1$, their curves with and without estimation of interference effects are almost the same. Our calculations agree better with the experiments given by Brion *et al* [3] whereas the ones obtained with Dyson orbitals are in general accordance with the ones reported by Truesdale [5]. We remark that our cross sections give a proper continuation of the calculations by Gozem *et al* [1] at high photon energies. In particular, our predictions agree well with the experiments at high impact energies around 100 eV by Banna *et al* [6] where there is a lack of theoretical results.

In figure 2(d), we show our results for the $3a_1$ orbital together with other predictions and experiments. Our cross sections are computed with $Z_{ef}^{O} = 2.0792$ and $Z_{ef}^{H_{a,b}} = 1.0392$, obtaining a very good agreement with the experiments. As can be seen, the calculations by Gozem *et al* [1] employing the CC model with Dyson orbitals and an $Z_{ef} = 1$ overestimate the measurements. In general, the results by Hilton *et al* [25] present discrepancy with our curves and the experiments. On the contrary, the cross sections by Stener *et al* [2] give a better description. The LB94 GS and TS calculations tend to underestimate the experimental results whereas the VWN TS ones agree well with the measurements by Tan *et al* [4] up to approximately 50 eV. The VWN GS model agrees well with the experiments by Banna *et al* [6] at

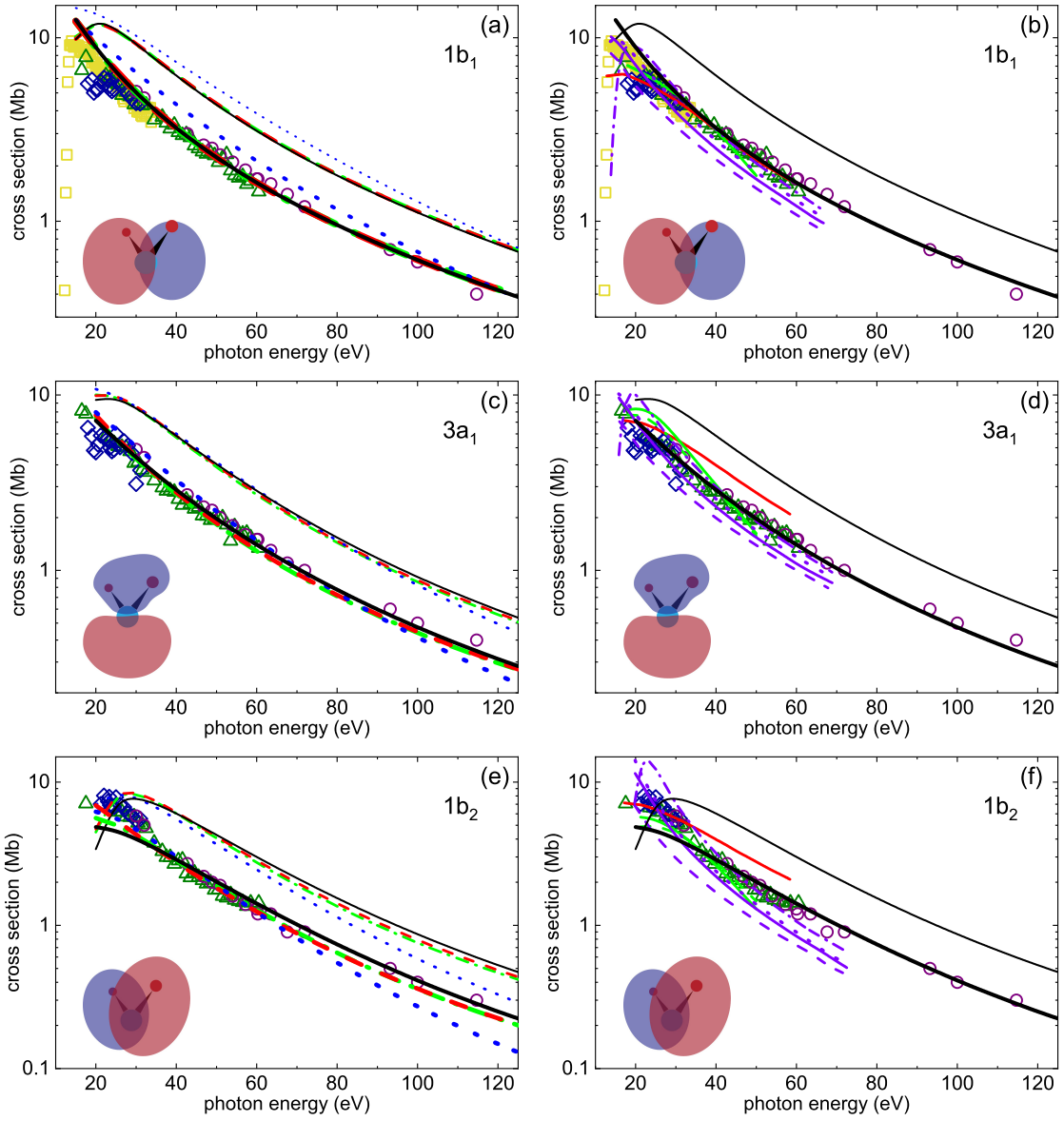

Figure 2: Total cross sections (σ^j) as a function of the photon energy for photoionization of several water orbitals . Present results: basis set IV, Belkić's distorted charge (——) and asymptotic charge (——); basis set III, Belkić's distorted charge (– – –) and asymptotic charge (– – –); basis set II, Belkić's distorted charge (– · – · –) and asymptotic charge (– · · – · · –) ; basis set I, Belkić's distorted charge (· · · · · ·) and asymptotic charge values (· · · · · ·). In (b), (d) and (f) calculations from [25] with (——) and without (– – –) estimation of interference effects, from [1] (——) and from [2] for LB94 GS (——), LB94 TS (– – –), VWN GS (– · – · –) and VWN TS (· · · · · ·). Experiments: [3] (□), [4] (△), [5] (◊) and [6] (◯).

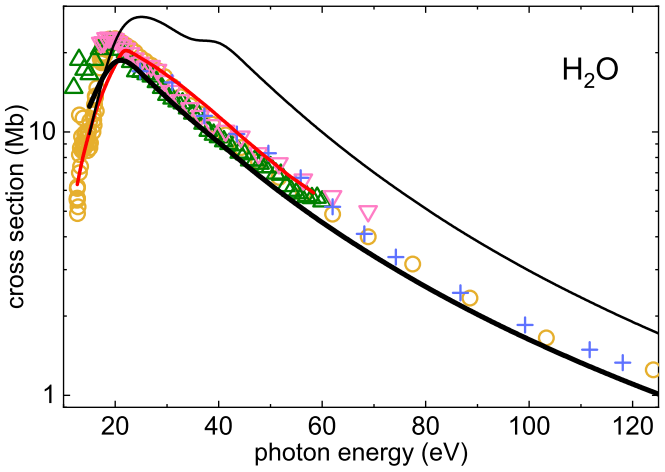

Figure 3: Total cross sections (σ) as a function of the photon energy for photoionization of water. Present results: basis set IV with Belkić's distorted charge (——) and asymptotic charge (——). Calculations from [1] (——). Experiments: [4] (△), [7] (◯), [8] (+) and [9] (▽).

low energies and with the results by Tan *et al* [4] for energies greater than 45 eV and about 40-50 eV are very close to our predictions that give the correct trend for the results by Banna *et al* [6] where there exist a lack of theoretical results.

A similar situation is observed for the $1b_2$ orbital in figure 2(f), where we show our results obtained with $Z_{ef}^{O} = 2.3264$ and $Z_{ef}^{H_{a,b}} = 1.1632$ along with other theories and experiments. Again, our cross sections reproduce very well the experimental results by Banna *et al* [6] for photon energies greater than 70 eV where no theoretical cross sections are available. The calculations by Gozem *et al* [1], that overestimate the measurements, agree qualitatively well with our results presenting almost the same slope. However, the calculations by Stener *et al* [2] and by Hilton *et al* [25] present discrepancies.

Finally, in figure 3, we present our total cross sections for water obtained summing the contribution of the previous relevant orbitals at the photon energies considered. We observe that the present results computed with the basis set IV and Belkić's charges as well as the ones by Gozem *et al* [1] are in general agreement for experiments at low photon energies. In addition, our predictions are in very good agreement with the measurements of Haddad *et al* [7] and Reilhac *et al* [8] at high photon energy.

3.1.1. Coherent emission and interference effects

After obtaining a very good agreement with our predictions using the more elaborated basis set for the bound orbitals of water and distorted charges by using the Belkic's criterion for the continuum final states, we are in position to analyze if the coherent emission plays a role in the total cross sections. As is well established [18],

interferences effects coming from the coherent emission from the different centers of the molecule are not easily detected in total cross sections as they decrease quickly with increasing energy. In order to isolate the effect of the interferences, one can rewrite the $\sigma^j(\omega)$ molecular total cross section averaged over all orientations and for a definite water orbital given by (13) as,

$$\sigma^j(\omega) = \sigma^j_{eff}(\omega)\ F^j(\omega), \tag{15}$$

with

$$F^j(\omega) = \frac{\sigma^j(\omega)}{\sigma^j_{eff}(\omega)}, \tag{16}$$

where $\sigma^j_{eff}(\omega)$ is an effective monocentric cross section corresponding to an incoherent sum of the cross sections of the atomic components of the molecule considered as incoherent emissors. In this way, the cross section of the molecule is obtained as a product of an effective atomic cross section times an interference factor F^j. This factor isolates the interference effects and gives information on the coherent emission from the different centers of the molecule [18]. In previous works, the effective atomic cross section were obtained as a sum of effective atomic cross sections with effective charges for the target bound states [18]. In this work, we obtain these effective atomic cross sections for the different orbitals by using the CNDO approximation [16]. The weights corresponding to the coefficients of the linear combinations that account for the atomic character present in each molecular orbital in this approximation are given in table C1 of Appendix C. Therefore, the effective total cross sections for the different water molecule orbitals by using the CNDO approximation are obtained as,

$$\sigma^j_{eff}(\omega) = \sum_i a^j_i\ \sigma_i\left(Z^i_{ef}\right), \tag{17}$$

with $i = H_{1s}, O_{1s}, O_{2s}, O_{2p}$. The coefficients a^j_i are specified in table C1 of Appendix C and we have used, for calculations of the individual atomic orbitals total cross sections σ_i, initial atomic i-states developed on a basis of STO (7) by a *Roothaan-Hartree-Fock* method (RHF) [26]. Besides, we consider distorted charges for the continuum obtained with the Belkić's rule [21] $Z^i_{ef} = \sqrt{2n_i^2|E^i_b|}$, where n_i is the quantum number of the atomic orbital and E^i_b is the orbital energy from the RHF method ($Z^{H_{1s}}_{ef} = 1$, $Z^{O_{2s}}_{ef} = 3.1551$, $Z^{O_{2p}}_{ef} = 2.2484$).

In figures 4 and 5, we present results for the $3a_1$ and $1b_2$ orbitals, respectively, that are expected to present three-centers interference effects considering their ligand character. As a fact, we observe in figures 4(a) and 5(a) that the molecular cross sections as a function of the energy present deviations from effective atomic ones obtained with the CNDO approximation (17) as the photon energy increases. These differences may be attributed to the coherent emission from the centers of the molecule. This can be seen in the corresponding interference factors F^j shown in figures 4(b) and 5(b). The interference factor deviates considerably from unity

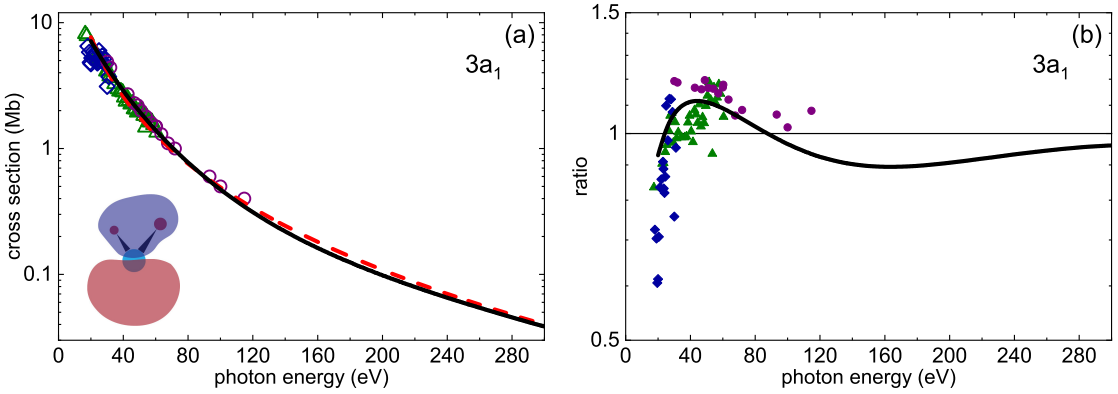

Figure 4: (a) Total cross sections as a function of the photon energy for photoionization of the $3a_1$ water orbital ($\sigma^j(\omega)$) with basis set IV for Belkić's distorted charge (——), effective monocentric cross section averaged over the atomic magnetic sub-levels ($\sigma^j_{eff}(\omega)$) (– – –) and experiments from [4] (△), [5] (◊) and [6] (◯). (b) $F^j(\omega)$ ratio (——) and ratio between the experimental data and the effective monocentric cross sections for [4] (▲), [5] (◆) and [6] (●).

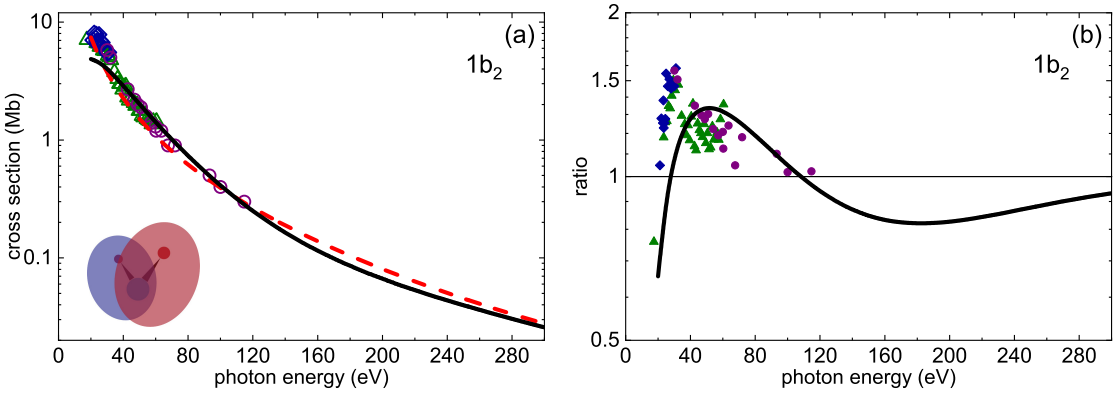

Figure 5: Same as figure 4 for the $1b_2$ water orbital.

as a function of the photon energy showing a typical oscillatory behavior [18]. We observe that our predictions for F^j are in good qualitative agreement with the ratio of the available experimental results to the effective atomic cross sections also shown in the figures. The deviations from unity of F^j for the $1b_2$ orbital are significantly greater than the ones of the $3a_1$ orbital. This may be explained considering that the electronic density of the $1b_2$ orbital is more delocalized over the three centers of the molecule [27].

To have a complete contrast of our predictions for the F^j factor, experiments at higher energies are needed. However, we recall that the interference effects could be detected also in the angular distributions (AD) [28, 18]. Consequently, we present first in figure 6 AD for the $3a_1$ orbital at 50 eV photon impact energy for several molecule orientations. The evolution of the AD exhibits an interesting behavior especially in figure 6(c) where many lobes appear. However, the intensity of this

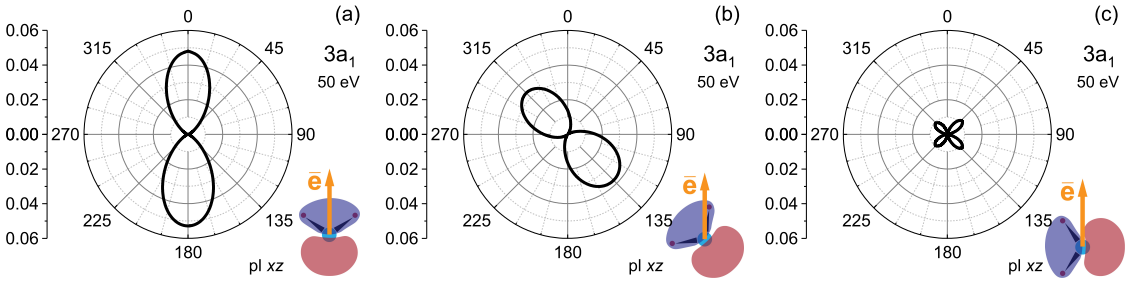

Figure 6: Angular distributions for photoionization from the $3a_1$ water orbital at different molecule orientations. Photon energy of 50 eV and Belkić's distorted charge charge. Polarization vector parallel to the z axis.

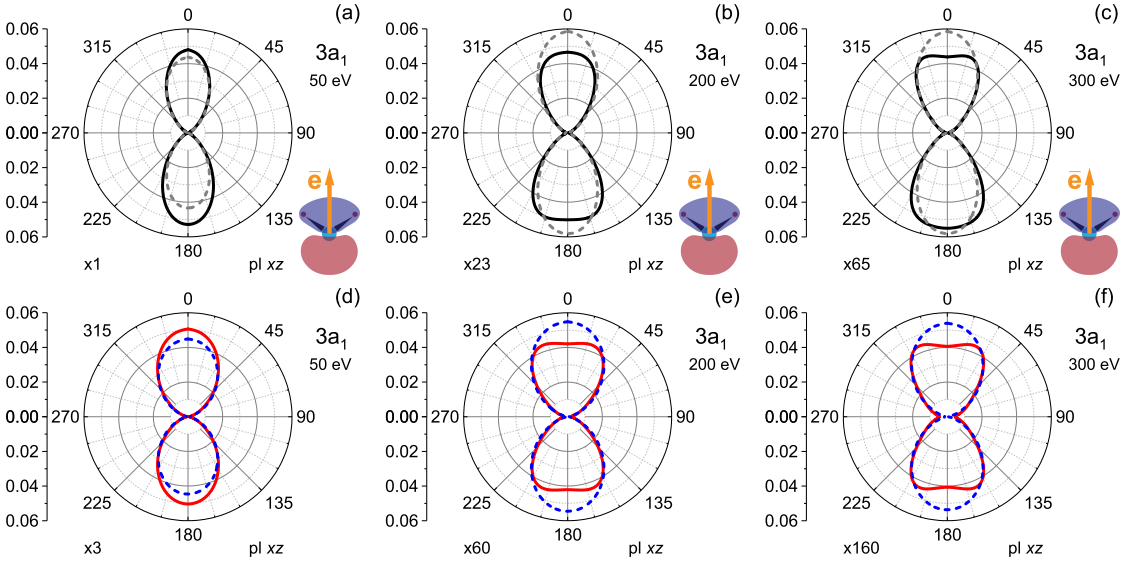

Figure 7: Angular distributions for the $3a_1$ water orbital at different photon energies with Belkić's distorted charge. Results for fixed (——) and randomly oriented molecules (——). CNDO calculations with and without average over the atomic magnetic sub-levels (– – –) and (– – –), respectively.

arrangement is clearly less than the one observed in figure 6(a) where the polarization vector bisects the HOH angle. Besides, the simultaneous obtention of the AD and the determination of the molecule orientation, although in principle accesible through COLTRIMS arrangements, is still a difficult experimental task. So, we show in figure 7, AD averaged over all molecular orientations for the $3a_1$ orbital at 50, 200 and 300 eV photon energies. Comparing figure 6(a) with figure 7(a) (both at 50 eV photon energy), we can see that the averaged AD are similar in shape to the ones corresponding to the molecular orientation shown in figure 6(a).

Then, this orientation seems to be the dominant one. Moreover, we show in the figure AD averaged over all orientations obtained with the CNDO approximation. As the CNDO is a monocentric approximation, the corresponding AD cannot exhibit

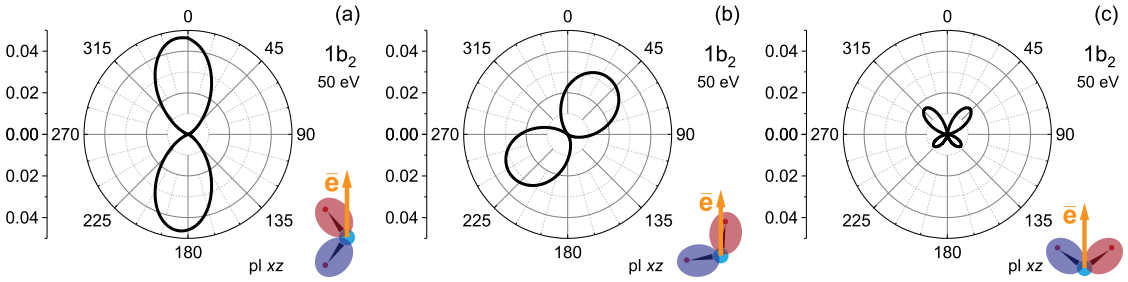

Figure 8: Same as figure 6 for the $1b_2$ water orbital.

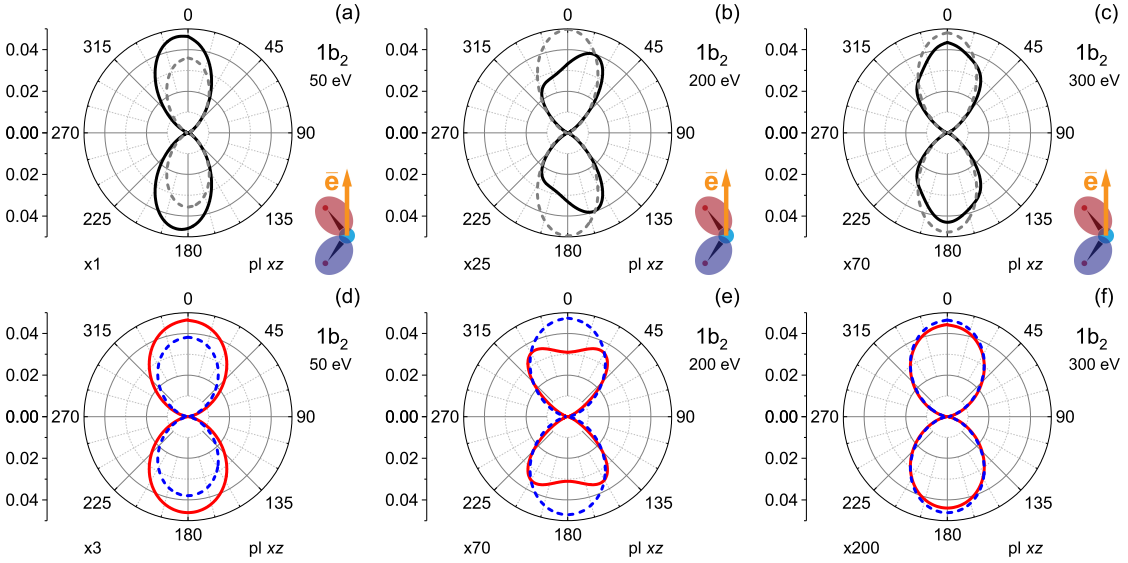

Figure 9: Same as figure 7 for the $1b_2$ water orbital.

interference effects coming from the multicenter nature of the molecule. As the energy increases, it is observed that the molecular AD present a clear decrease in the classical emission direction given by the polarization vector that is not present in the monocentric AD. This is a clear trace of the interference effects provoked by the coherent emission from the centers of the molecule. A similar scenario is observed for the $1b_2$ orbital. In figure 8 we show AD for several molecule orientations at 50 eV photon impact energy. In this case, the orientation depicted in figure 8(c) appears as the dominant one. This can be checked in figure 9(a), where we show AD averaged over all orientations at 50 eV photon energy. As can be seen, the shape of the averaged AD are similar to the ones presented in figure 8(a). Then, in figure 9 we compare averaged molecular AD and monocentric ones at 50, 200 and 300 eV photon energies. Again, we see that the averaged molecular AD at 200 eV present a partial suppression of the photoelectron emission in the classical direction given by the polarization vector.

Finally, we revisit in figure 10 the AD for the $1b_2$ orbital shown in figure 9(b) where the interference effects are more evident than in the case of the $3a_1$ orbital.

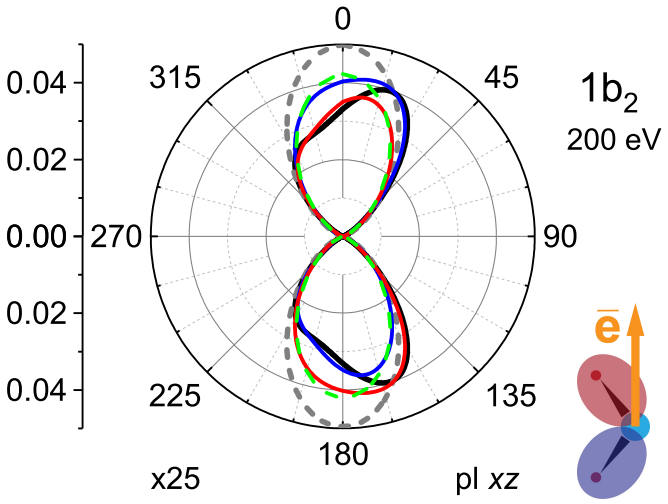

Figure 10: Same as figure 9(b). Model calculations: $g_1 = 1$ (——), $g_2 = 1$ (——) and $g_1 = g_2 = 1$ (– – –) in (8) .

However, the following conclusion are analogous for this orbital. In figure 10, we show additional model calculations of AD for a ficticious molecule where we replace in (8) the g_i traslational factors corresponding to either $H_{a,b}$ center by unity. We can observe that the AD of the molecule are considerably altered when the g_i factor of any $H_{a,b}$ is omitted (i.e., when $g_1 = 1$ or, alternatively, $g_2 = 1$). If both factors are omitted (i.e., when $g_1 = g_2 = 1$), no suppression at all of the emission in the classical direction given by the polarization vector is observed. Then, this simple calculations show unambiguously that the interferences detected in the AD are the result of coherent emission coming from the three centers of the molecule acting all together in a coherent way.

4. Conclusions

We have studied photoemission from water through a model with low computational cost but able to take into account the three-center geometry of the molecule. We have analyzed in detail the effect of the coherent emission from either center of the molecule. We have computed photoionization total cross sections as a function of the photon energy within the dipole approximation in the energy range [20,300] eV. We obtain very good agreement with more elaborated previous results as well as with experiments. In particular, our results agree very well with the available experiments in the region of high enough photon energy where there is a lack of theoretical predictions. In this sense, our work aims at fill a gap providing accurate cross sections in this region. Moreover, we have revealed interference effects in the total cross sections coming from the coherent emission from the centers of the molecule. In addition, we have put in evidence that interferences coming from the coherent emission phenomena may be observed in the ratios between total

cross sections and effective monocentric cross sections. We have shown that these interferences could be detected not only in the total cross sections but also in the angular distributions of photoelectrons for randomly oriented molecules. Then, the trace of the coherent emission may be inferred without need of any other adequate observable (such as the effective cross sections used to obtain ratios). Besides, we show that in certain situations, emission of photoeletrons in the classical direction given by the polarization vector is partially forbidden. The basic physical mechanism underlying this suppression is the (partial destructive) interference produced by the coherent emission from the centers of the molecule. Then, this suppression will depend critically on the photoelectron energy and the ejection direction. We think that our results may be useful in several domains. On one hand, our cross sections may be employed as the basic inputs to fed Monte Carlo codes to obtain the energy deposition in the biological medium. On the other hand, new experimental results are needed to check our predictions about interference effects in the angular distributions. In this sense, our work may promote the design of new basic experiments with high energy photons interacting with molecules employing the new radiation sources such as the intense XUV pulsed lasers and XFEL installations [29].

Acknowledgments

Authors acknowledge financial support from the Agencia Nacional de Promoción Científica y Tecnológica (PICT No. 01912)2015-3392 and the Consejo Nacional de Investigaciones Científicas y Técnicas de la República Argentina (PIP No. 11220090101026).

Appendix A

We obtain the matrix transition element for a definite initial orbital of water ψ^j (given by (6)) within the framework of an effective center approximation [18].

By taking $\psi_b = \psi^j$ in (1) we get,

$$M_{ph}^j = -\mathrm{i}\langle\psi_f|\mathbf{e}\cdot\nabla|\sum_i\sum_\mu^{\mathbb{N}} c_{i\mu}^j f_\mu(\mathbf{r}_i')\rangle, \tag{A.1}$$

that can be rewritten as,

$$M_{ph}^j = \sum_i M_{ph}^{j,i}, \tag{A.2}$$

where we define,

$$M_{ph}^{j,i} = -\mathrm{i}\langle\psi_f|\mathbf{e}\cdot\nabla|\sum_\mu^{\mathbb{N}} c_{i\mu}^j f_\mu(\mathbf{r}_i')\rangle. \tag{A.3}$$

In the last expression, the final wavefunction ψ_f describes the asymptotic final state of the electron under the influence of the Coulomb field of the charged residual target.

In order to simplify the calculations, we apply an effective center approximation [18]. Then, to evaluate each matrix element given by (A.3), the hypergeometric function appearing in the final wavefunction is evaluated at the center labelled i.

Then, for the center $i = O$, we have,

$$M_{ph}^{j,O} = -\mathrm{i} \int d\mathbf{r}'_0 \, (2\pi)^{-3/2} e^{-\mathrm{i}\mathbf{k}_e \cdot \mathbf{r}'_0} N_{k_e}^* G^*(\mathbf{r}'_0) \, (\mathbf{e} \cdot \nabla) \sum_{\mu}^{\mathbb{N}} \, c_{O\mu}^j f_\mu \, (\mathbf{r}'_0) \, , \tag{A.4}$$

and for the centers $i = H_a, H_b$ we have, respectively,

$$M_{ph}^{j,H_a} = -\mathrm{i} \int d\mathbf{r}'_1 \, (2\pi)^{-3/2} e^{-\mathrm{i}\mathbf{k}_e \cdot \mathbf{r}'_0} N_{k_e}^* G^*(\mathbf{r}'_1) \, (\mathbf{e} \cdot \nabla) \sum_{\mu}^{\mathbb{N}} \, c_{H_a\mu}^j f_\mu \, (\mathbf{r}'_1) \, , \tag{A.5}$$

$$M_{ph}^{j,H_b} = -\mathrm{i} \int d\mathbf{r}'_2 \, (2\pi)^{-3/2} e^{-\mathrm{i}\mathbf{k}_e \cdot \mathbf{r}'_0} N_{k_e}^* G^*(\mathbf{r}'_2) \, (\mathbf{e} \cdot \nabla) \sum_{\mu}^{\mathbb{N}} \, c_{H_b\mu}^j f_\mu \, (\mathbf{r}'_2) \, . \tag{A.6}$$

Now, taking into account that $\mathbf{r} \equiv \mathbf{r}'_0 = \mathbf{r}_{1,2} + \mathbf{r}'_{1,2}$, we obtain,

$$M_{ph}^{j,H_a} \sim -\mathrm{i} e^{-\mathrm{i}\mathbf{k}_e \cdot \mathbf{r}_1} \int d\mathbf{r}'_1 \, (2\pi)^{-3/2} e^{-\mathrm{i}\mathbf{k}_e \cdot \mathbf{r}'_1} N_{k_e}^* G^*(\mathbf{r}'_1) \, (\mathbf{e} \cdot \nabla) \times \\ \times \sum_{\mu}^{\mathbb{N}} \, c_{H_a\mu}^j f_\mu \, (\mathbf{r}'_1) \, , \tag{A.7}$$

$$M_{ph}^{j,H_b} \sim -\mathrm{i} e^{-\mathrm{i}\mathbf{k}_e \cdot \mathbf{r}_2} \int d\mathbf{r}'_2 \, (2\pi)^{-3/2} e^{-\mathrm{i}\mathbf{k}_e \cdot \mathbf{r}'_2} N_{k_e}^* G^*(\mathbf{r}'_2) \, (\mathbf{e} \cdot \nabla) \times \\ \times \sum_{\mu}^{\mathbb{N}} \, c_{H_b\mu}^j f_\mu \, (\mathbf{r}'_2) \, . \tag{A.8}$$

Finally,

$$M_{ph}^{j} \sim M_{ph}^{j,O} + e^{-\mathrm{i}\mathbf{k}_e \cdot \mathbf{r}_1} M_{ph}^{j,H_a} + e^{-\mathrm{i}\mathbf{k}_e \cdot \mathbf{r}_2} M_{ph}^{j,H_b} . \tag{A.9}$$

Appendix B

We present the obtention of the analytical expressions for the matrix transition elements for an initial state described by a unique STO.

Within the framework of the dipole approximation, the matrix element reads,

$$M_{ph} = -\mathrm{i} \langle \psi_f | \mathbf{e} \cdot \nabla | \psi_b \rangle , \tag{B.10}$$

where ψ_b is the initial electronic bound state, ψ_f is the final electronic state given by (2) and where $\mathbf{e}$ represent the polarization vector of the incident radiation.

As an example, we show the calculations for the transition matrix amplitude of the simplest Slater orbital, ϕ_{100} given by (7). In this case, the initial wavefunction ψ_b for the transition matrix element (B.10) is given by,

$$\psi_{\phi_{100}}(\mathbf{r}) = \frac{\xi^{3/2}}{\sqrt{\pi}} e^{-\xi r}. \tag{B.11}$$

Replacing (B.11) and (2) in (B.10), one obtains,

$$M_{\phi_{100}} = -\mathrm{i}\,(2\pi)^{-3/2}\, N_{k_e}^{*}\, \frac{\xi^{3/2}}{\sqrt{\pi}} \int d\mathbf{r}\; e^{-\mathrm{i}\mathbf{k}_e\cdot\mathbf{r}}\; G^{*}(\mathbf{r})\, \mathbf{e}\cdot\nabla\left(e^{-\xi r}\right). \tag{B.12}$$

Considering that $\nabla\left(e^{-\xi r}\right) = -\xi e^{-\xi r}\,\frac{\mathbf{r}}{r}$, one gets,

$$M_{\phi_{100}} = \mathrm{i}\,(2\pi)^{-3/2}\, N_{k_e}^{*}\, \frac{\xi^{5/2}}{\sqrt{\pi}} \int \frac{d\mathbf{r}}{r}\; e^{-\xi r-\mathrm{i}\mathbf{k}_e\cdot\mathbf{r}}\; G^{*}(\mathbf{r})\,(\mathbf{e}\cdot\mathbf{r}). \tag{B.13}$$

Now, if we consider the polarization versor $\mathbf{e}$ parallel to the z axis,

$$M_{\phi_{100}} = \mathrm{i}\,(2\pi)^{-3/2}\, N_{k_e}^{*}\, \frac{\xi^{5/2}}{\sqrt{\pi}} I_1, \tag{B.14}$$

where we have defined,

$$I_1 = \int \frac{d\mathbf{r}}{r}\; e^{-\xi r-\mathrm{i}\mathbf{k}_e\cdot\mathbf{r}}\; G^{*}(\mathbf{r})\, r_z, \tag{B.15}$$

with r_z the z-component of the position vector $\mathbf{r}$.

To solve this integral, we introduce a vector $\mathbf{v}$ parallel to the z axis and we define the integral,

$$I_2 = \int \frac{d\mathbf{r}}{r}\; e^{-\xi r-\mathrm{i}\mathbf{k}_e\cdot\mathbf{r}}\; e^{\mathrm{i}\mathbf{v}\cdot\mathbf{r}}\; G^{*}(\mathbf{r}) = \int \frac{d\mathbf{r}}{r}\; e^{-\xi r-\mathrm{i}\mathbf{k}_e\cdot\mathbf{r}}\; e^{\mathrm{i}vr_z}\; G^{*}(\mathbf{r}), \tag{B.16}$$

which satisfies,

$$I_1 = -\mathrm{i}\frac{\partial}{\partial v}\left(I_2\right)_{v=0}. \tag{B.17}$$

Therefore,

$$M_{\phi_{100}} = (2\pi)^{-3/2}\, N_{k_e}^{*}\, \frac{\xi^{5/2}}{\sqrt{\pi}} \frac{\partial}{\partial v}\left(I_2\right)_{v=0}. \tag{B.18}$$

Then, employing the Nordsieck's method [30], it is possible to approximate the integral I_2 as,

$$J(\lambda,\mathbf{q},\mathbf{v}) = \int \frac{d\mathbf{r}}{r}\; e^{-\lambda r+\mathrm{i}(\mathbf{q}+\mathbf{v}-\mathbf{p})\cdot\mathbf{r}}\; G^{*}(\mathbf{r}) = 4\pi\; f(\lambda,\mathbf{q},\mathbf{v}), \tag{B.19}$$

where,

$$f(\lambda,\mathbf{q},\mathbf{v}) = \frac{\left[(\mathbf{q}+\mathbf{v})^2 + (\lambda-\mathrm{i}p)^2\right]^{-\mathrm{i}\nu}}{\left[\lambda^2 + (\mathbf{q}+\mathbf{v}-\mathbf{p})^2\right]^{1-\mathrm{i}\nu}}. \tag{B.20}$$

Consequently,

$$I_2 = 4\pi f(\xi,\mathbf{0},\mathbf{v}), \tag{B.21}$$

with $\mathbf{p} = \mathbf{k}_e$ and the transition matrix element,

$$M_{\phi_{100}} = \frac{\sqrt{2}}{\pi} N^*_{k_e} \xi^{5/2} \frac{\partial}{\partial v} f(\xi, \mathbf{0}, \mathbf{v})_{v=0, \mathbf{p}=\mathbf{k}_e} \,. \tag{B.22}$$

Finally, calculating the derivative according to (B.22), we obtain the transition matrix element corresponding to the $1s$ Slater orbital,

$$M_{\phi_{100}} = \frac{2\sqrt{2}}{\pi} N^*_{k_e} \xi^{5/2} \frac{(1 - \mathrm{i}\nu)\,(\mathbf{e} \cdot \mathbf{k}_e)}{\left(\xi^2 + p^2\right)^2} e^{-2\nu\, arctg(k_e/\xi)}. \tag{B.23}$$

The matrix elements for other Slater orbitals can be computed in an analogous way. Those corresponding to the Slater orbitals ϕ_{200} and ϕ_{210} are given by, respectively,

$$\begin{aligned} M_{\phi_{200}} = {} & 2\sqrt{\frac{2}{3}} \frac{1}{\pi} N^*_{k_e} \xi^{5/2} \frac{(1 - \mathrm{i}\nu)\,(\mathbf{e} \cdot \mathbf{k}_e)}{\left(\xi^2 + k_e^2\right)^2} \times \\ & \times \left[\frac{3\xi^2 - k_e^2 - 2\nu\xi k_e}{\left(\xi^2 + k_e^2\right)} \right] e^{-2\nu\, arctg(k_e/\xi)}, \end{aligned} \tag{B.24}$$

and,

$$\begin{aligned} M_{\phi_{210}} = {} & \frac{2\sqrt{2}}{\pi} \mathrm{i} N^*_{k_e} \xi^{5/2} \left[\frac{\mathrm{i}\nu\xi(\xi + \mathrm{i}k_e)^2}{\left(\xi^2 + k_e^2\right)^3} - \frac{2\xi\,(2 - \mathrm{i}\nu)\,(1 - \mathrm{i}\nu)\,(\mathbf{e} \cdot \mathbf{k}_e)^2}{\left(\xi^2 + k_e^2\right)^3} + \right. \\ & \left. + \frac{\nu k_e - \xi}{\left(\xi^2 + k_e^2\right)^2} + \frac{\xi\,(1 - \mathrm{i}\nu)}{\left(\xi^2 + k_e^2\right)^2} \right] e^{-2\nu\, arctg(k_e/\xi)}. \end{aligned} \tag{B.25}$$

Appendix C

Table C1: Atomic percentages a_i^j (normalized to unity) of the molecular orbitals of water vapor obtained with the CNDO method.

i \ j	$1a_1$	$2a_1$	$1b_2$	$3a_1$	$1b_1$
O $2p$	-	-	0.59	0.73	1.00
$2s$	-	0.75	-	0.10	-
$1s$	1.00	-	-	-	-
H $1s$	-	0.25	0.41	0.17	-

References

[1] Gozem S, Gunina A O, Ichino T, Osborn D L, Stanton J F and Krylov A I 2015 *J. Phys. Chem. Lett.* **6** 4532

[2] Stener M, Furlan S and Decleva P 2000 *J. Phys. B: At. Mol. Opt. Phys.* **33** 1081

[3] Brion C E and Carnovale F 1985 *Chem. Phys.* **100** 291

[4] Tan K H, Brion C E, Van der Leeuw Ph E and Van der Wiel M J 1978 *Chem. Phys.* **29** 299

[5] Truesdale C M, Southworth S, Kobrin P H, Lindle D W, Thornton G and Shirley D A 1982 *J. Chem. Phys.* **76** 860

[6] Banna M S, McQuaide B H, Malutzki R and Schmidt V 1986 *J. Chem. Phys.* **84** 4739
[7] Haddad G N and Samson J A R 1986 *J. Chem. Phys.* **84** 6623
[8] de Reilhac L and Damany N 1977 *J. Quant. Spectrosc. Radiat. Transfer* **18** 121
[9] Phillips E, Lee L C and Judge D L 1977 *J. Quant. Spectrosc. Radiat. Transfer* **18** 309
[10] Yamazaki M, Adachi J, Teramoto T, Yagishita A, Stener M and Decleva P 2009 *J. Phys. B: At. Mol. Opt. Phys.* **42** 051001
[11] Kazama M, Shinotsuka H, Yamazaki M, Adachi J, Yagishita A and Fujikawa T 2009 *J. Phys. Conference Series* **190** 012048
[12] Fojón O A, Fernández J, Palacios A, Rivarola R D and Martín F 2004 *J. Phys. B: At. Mol. Opt. Phys.* **37** 3035
[13] Fojón O A, Palacios A, Fernández J, Rivarola R D and Martín F 2006 *Phys. Lett. A* **350** 371
[14] Tachino C A, Monti J M, Fojón O A, Champion C and Rivarola R D 2014 *J. Phys. B: At. Mol. Opt. Phys.* **47** 035203
[15] de Sanctis M L, Politis M-F, Vuilleumier R, Stia C R and Fojón O A 2015 *J. Phys. B: At. Mol. Opt. Phys.* **48** 155201
[16] Pople J A and Segal G A 1965 *J. Chem. Phys.* **43** 5136
[17] Martini L, Boll D I R and Fojón O A 2017 *Papers in Physics* **9** 090006
[18] Ciappina M F, Fojón O A and Rivarola R D 2014 *J. Phys. B: At. Mol. Opt. Phys.* **47** 042001
[19] Boll D I R and Fojón O A 2014 *Phys. Rev. A* **90** 053414
[20] Boll D I R and Fojón O A 2016 *J. Phys. B: At. Mol. Opt. Phys.* **49** 185601
[21] Belkić Dž, Gayet R and Salin A 1979 *Phys. Rep.* **56** 279
[22] Siegbahn K, Nordling C, Johansson G, Hedman J, Heden P F, Hamrin K, Gelius U, Bergmark T, Werme L O, Manne R and Baer Y (eds) 1969 *ESCA applied to free molecules* (North-Holland Publishing Company)
[23] Aung S, Pitzer R M and Chan S I 1968 *J. Chem. Phys.* **49** 2071
[24] Yudin G L, Patchkovskii S and Bandrauk A D 2006 *J. Phys. B: At. Mol. Opt. Phys.* **39** 1537
[25] Hilton P R, Nordholm S and Hush N S 1979 *Chem. Phys. Lett.* **64** 515
[26] Clementi E and Roetti C 1974 *At. Data Nucl. Data Tables* **14** 177
[27] Dunning T H, Pitzer R M and Aung S 1972 *J. Chem. Phys.* **57** 5044
[28] Fernández J, Fojón O, Palacios A and Martín F 2007 *Phys. Rev. Lett.* **98** 043005
[29] Yagishita A 2015 *J. Electron Spectros. Relat. Phenomena* **200** 247
[30] Nordsieck A 1954 *Phys. Rev.* **93** 785